NAVAL POSTGRADUATE SCHOOL

MONTEREY, CALIFORNIA

THESIS

DIRECT NUMERICAL SIMULATIONS OF DIFFUSIVE STAIRCASES IN THE ARCTIC

by

Gregory P. Caro

March 2009

Thesis Advisor: Timour Radko
Second Reader: Jeff Haferman

Approved for public release; distribution is unlimited

THIS PAGE INTENTIONALLY LEFT BLANK

REPORT DOCUMENTATION PAGE		Form Approved OMB No. 0704-0188

1. AGENCY USE ONLY *(Leave blank)*	2. REPORT DATE	3. REPORT TYPE AND DATES COVERED
	March 2009	Master's Thesis

4. TITLE AND SUBTITLE	5. FUNDING NUMBERS
Direct Numerical Simulations of Diffusive Staircases in the Arctic.	
6. AUTHOR(S) Gregory P. Caro	
7. PERFORMING ORGANIZATION NAME(S) AND ADDRESS(ES) Naval Postgraduate School Monterey, CA 93943-5000	**8. PERFORMING ORGANIZATION REPORT NUMBER**
9. SPONSORING /MONITORING AGENCY NAME(S) AND ADDRESS(ES) N/A	**10. SPONSORING/MONITORING AGENCY REPORT NUMBER**

11. SUPPLEMENTARY NOTES
The views expressed in this thesis are those of the author and do not reflect the official policy or position of the Department of Defense or the U.S. Government.

12a. DISTRIBUTION / AVAILABILITY STATEMENT	12b. DISTRIBUTION CODE
Approved for public release; distribution is unlimited	

13. ABSTRACT (maximum 200 words)

The vertical transport of heat by the diffusive layer in the Arctic thermocline is a critical element of the high-latitude climate, and yet, after decades of research, the extant estimates remain highly controversial. Laboratory-based estimates of vertical heat fluxes originating from the thermohaline staircases of the thermocline are typically on the order of $0.1 W/m^2$. This study suggests that these laboratory experiments underestimate the vertical heat fluxes and exceed their calculations by nearly an order of magnitude.

We first quantify the typical density ratio, step height and temperature gradient within the diffusive staircases of the Beaufort Gyre. Then, these characteristics are used as an input into a numerical model, which simulates the vertical heat fluxes driven by the double diffusive processes. The series of two-dimensional simulation runs consistently calculated heat fluxes on the order of $1 W/m^2$. In addition, analysis of a three-dimensional simulation suggests that the three-dimensional fluxes substantially exceed their two-dimensional counterparts. A detailed analysis of the laboratory measurements suggests that the empirical coefficients estimated scaling factors from these experiments are inconsistent with the corresponding numerical simulations. These findings suggest that laboratory derived flux laws cannot be directly applied to the Arctic Ocean and that further investigations into double-diffusive convective processes are warranted.

14. SUBJECT TERMS	15. NUMBER OF PAGES
Double-diffusion, diffusive convection, heat flux, thermohaline staircase,	61
	16. PRICE CODE

17. SECURITY CLASSIFICATION OF REPORT	18. SECURITY CLASSIFICATION OF THIS PAGE	19. SECURITY CLASSIFICATION OF ABSTRACT	20. LIMITATION OF ABSTRACT
Unclassified	Unclassified	Unclassified	UU

NSN 7540-01-280-5500 Standard Form 298 (Rev. 2-89)
Prescribed by ANSI Std. 239-18

THIS PAGE INTENTIONALLY LEFT BLANK

Approved for public release; distribution is unlimited

DIRECT NUMERICAL SIMULATIONS OF DIFFUSIVE STAIRCASES IN THE ARCTIC

Gregory P. Caro
Lieutenant Commander, United States Navy
B.S., University of Southern California, 1993

Submitted in partial fulfillment of the
requirements for the degree of

MASTER OF SCIENCE IN PHYSICAL OCEANOGRAPHY

from the

NAVAL POSTGRADUATE SCHOOL
March 2009

Author: Gregory P. Caro

Approved by: Timour Radko
Thesis Advisor

Jeff Haferman
Second Reader

Jeff Paduan
Chairman, Department of Oceanography

THIS PAGE INTENTIONALLY LEFT BLANK

ABSTRACT

The vertical transport of heat by the diffusive layer in the Arctic thermocline is a critical element of the high-latitude climate, and yet, after decades of research, the extant estimates remain highly controversial. Laboratory-based estimates of vertical heat fluxes originating from the thermohaline staircases of the thermocline are typically on the order of $0.1 W/m^2$. This study suggests that these laboratory experiments underestimate the vertical heat fluxes and exceed their calculations by nearly an order of magnitude.

We first quantify the typical density ratio, step height and temperature gradient within the diffusive staircases of the Beaufort Gyre. Then, these characteristics are used as an input into a numerical model, which simulates the vertical heat fluxes driven by the double diffusive processes. The series of two-dimensional simulation runs consistently calculated heat fluxes on the order of $1 W/m^2$. In addition, analysis of a three-dimensional simulation suggests that the three-dimensional fluxes substantially exceed their two-dimensional counterparts. A detailed analysis of the laboratory measurements suggests that the empirical coefficients estimated scaling factors from these experiments are inconsistent with the corresponding numerical simulations. These findings suggest that laboratory derived flux laws cannot be directly applied to the Arctic Ocean and that further investigations into double-diffusive convective processes are warranted.

THIS PAGE INTENTIONALLY LEFT BLANK

TABLE OF CONTENTS

THIS PAGE INTENTIONALLY LEFT BLANK

LIST OF FIGURES

THIS PAGE INTENTIONALLY LEFT BLANK

LIST OF TABLES

THIS PAGE INTENTIONALLY LEFT BLANK

ACKNOWLEDGMENTS

I would like to thank Dr. Timour Radko for his infinite patience and ability to make difficult concepts easy to understand. His devotion to his work and general concern for his students made him an excellent thesis advisor and mentor. I would also like thank Mike Cook for his unending help and expertise with Matlab and general coding issues. He helped turn ten-hour debugging processes into one-hour productive script writing. My thanks also goes out to Jeff Haferman for giving my thesis the objective read and for also connecting me to various computer clusters in order to complete my calculations.

The last two years I spent away from my family, who lived in San Diego. I could not have achieved this goal if it were not for their support and understanding throughout this whole process. My wife spent the middle of the weeks as a single mom to our children, allowing me to study up here on my own without distraction. I know the words “Thank You” are not enough. And finally, to my children, who spent their school days without their father. I hope that they will one day equate this time away to how much their parents value a good education.

THIS PAGE INTENTIONALLY LEFT BLANK

I. INTRODUCTION

In the February 2009 issue of U.S. Naval Institute's *Proceedings Magazine*, Rear Admiral David Gove, U.S. Navy, began his article on Arctic Melt by stating "Changes in the Arctic environment — no matter the cause — are a great national security concern." He further asserted:

> To ensure complete maritime domain awareness in the region, and to provide our forces a competitive advantage, it will be necessary to have a comprehensive knowledge of the physical environment...Computer-based ocean and atmospheric models must be adjusted to the geophysical peculiarities of high latitudes.

In December 2007, the United States Environmental Protection Agency reported that warming rates in the Arctic will be the greatest of any other region in the world, due in part to the retreating of ice formations. Less ice on the surface of the ocean increases the amount of the sun's energy that is absorbed into the water column, thereby further warming the planet. Add to this scenario the possibility that the warmer Atlantic Deep Water sliding beneath the colder and fresher Upper Polar Deep Water (see Figure 1) can also convect enough energy to add to the demise of the Arctic sea ice.

A pronounced feature of the Arctic thermocline is related to the abundance of the double-diffusive structures in the region. The ultimate goal of this thesis is physically based parameterization and prediction of vertical double-diffusive heat fluxes. It is equally important to determine whether these fluxes are significant enough to affect the Arctic Climate. This study is based on a

combination of data analysis and numerical modeling. First, we quantify the typical density ratio, step height and temperature gradient within the diffusive staircases of the Beaufort Gyre. Then, the data are used as input into a numerical simulation, which simulates the vertical heat fluxes within the gyre due to double diffusive layering processes.

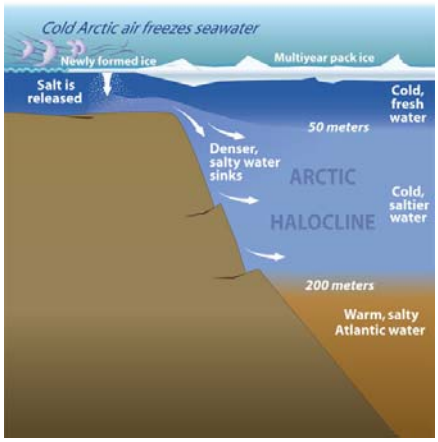

Figure 1. Cross section of Arctic water mass. Cold and relatively fresh water sits atop more warmer and saline Atlantic water. Illustration by Jayne Doucette, Woods Hole Oceanographic Institution. Obtained from WHOI ITP website: http://www.whoi.edu/oceanus/viewArticle

Despite the critical role played by the Arctic Ocean in the global climate, the vertical heat and salt fluxes through the main Arctic thermocline remain a source of greatest uncertainty. Do these fluxes have a role in the Arctic climate? In 1965, Turner derived his well-known 4/3 flux law based on dimensional analysis, which attempted to quantify heat flux, F_T:

$$\alpha F_T = C(R_\rho)\cdot\left(\frac{g\kappa_T^2}{\nu}\right)^{\frac{1}{3}}\cdot(\alpha\Delta T)^{\frac{4}{3}} \qquad (1)$$

where C is a function of R_ρ is the background density ratio, κ_T is the molecular diffusivity of heat, g is the gravitational acceleration, ν is the kinematic viscosity, α is the coefficient of thermal expansion, and ΔT is the temperature variation. Others would follow (Padman & Dillon, 1987; Marmarino & Caldwell, 1976; Kelley, 1990) and attempt to calibrate Turner's law with empirical data garnered from laboratory experiments.

The usual set up typically involves introducing a two-layer stratification (cold and fresh water on top of warm and salty) in the experimental tank and monitoring T and S variation in the layers. Conservation laws are then used to infer the temperature and salinity fluxes. One of the assumptions is that there are no heat losses to the sidewalls. Another and perhaps even more critical concern with this setup is the fact that the interaction between the lower layer and the tank bottom is not an adequate model for the layers in nature (Padman & Dillon, 1987). The rigid boundaries pose a hindrance to the convective mixing and as we argue here, results in a significant underestimation of the vertical transport. These attempts have been criticized as simplistic and prone to large errors and yielded estimates of the vertical heat flux in the staircase region on the order of $0.02 W/m^2$ to $0.22 W/m^2$. It has been noted that heat fluxes less that $1 W/m^2$ are not significant enough to affect the Arctic Ocean surface heat budget (Timmermans et al., 2008).

Numerical modeling is the simplest and most obvious tool for evaluating the mixing characteristics in the Arctic Ocean, and it will be extensively used in our study, supplemented by the analysis of relevant observations. Several attempts have already been made (Molemaker & Dijkstra, 1997; Prikasky, 2007) to address the problem numerically, but computational difficulties precluded simulations of the parameter regime relevant for the Arctic staircases. However, recent advances in high-performance computing make it possible now to perform: i) first three-dimensional simulation of the diffusive convection in the numerically accessible regime and ii) realistic two-dimensional simulations in the parameter range directly applicable to the Arctic staircases. The analysis in this thesis is based on both two-dimensional and three-dimensional models. A series of simulation runs are performed in which we systematically vary the background parameters, within the limits relevant for the Beaufort Gyre staircases, record and analyze the vertical heat fluxes and their dependencies.

This thesis is set up as follows. In Chapter II, we introduce the double-diffusive processes and discuss their dynamics. In Chapter III, we investigate the Beaufort Gyre and calculate the parameters characteristic of the Arctic location. Chapter IV discusses in depth the numerical model and quantifies heat fluxes calculated in both two-dimensions and three-dimensions. These fluxes are analyzed and compared with laboratory derived fluxes. Finally, our conclusions are drawn, and recommendations for future work in this field of study are offered.

II. DOUBLE-DIFFUSIVE CONVECTION: BACKGROUND

A. DOUBLE-DIFFUSIVE CONVECTION

Turner (1973) describes double-diffusive convection as a phenomenon that occurs when there are gradients of two or more properties with different molecular diffusivities. The double-diffusive instability represents an efficient mechanism that releases potential energy stored in one of the density components, even when the density distribution is statically stable. With regard to the ocean, net differences in the diffusivity of heat and salt are of interest. At 20 degrees Celsius the diffusivity of heat (κ_T = 1.49x10^{-7} m^2/s) is on the order of 100 times greater than that of salt (κ_S = 0.129x10^{-7} m^2/s). The disparity in diffusivities is even greater in the high latitude ocean (κ_T =1.39x10^{-7} m^2/s, κ_S =0.0068x10^{-7} m^2/s) (Kraus & Businger, 1994). There are two types of double-diffusion, which are known as the salt finger regime and the diffusive convection regime.

1. Salt Finger Regime

Salt fingers are usually observed in warm climates such as the tropics and subtropics, where the combination of evaporation and solar heating at the ocean surface results in a layer of warm, salty water atop relatively cooler and fresher water. The physical mechanism of salt fingering is illustrated in Figure 2. Imagine displacing a parcel of warm, salty water across the thin interface into a region of

colder and fresher water. Due to the higher diffusion rate of heat, the parcel of water quickly loses its heat to its new surrounding. At the same time, it diffuses salt to the less saline environment, but 100 times slower. As a result, the parcel of water remains saltier and therefore denser than the surrounding fluid and continues to sink further. This instability is manifested by the appearance of narrow and elongated vertical filaments, a.k.a. salt fingers.

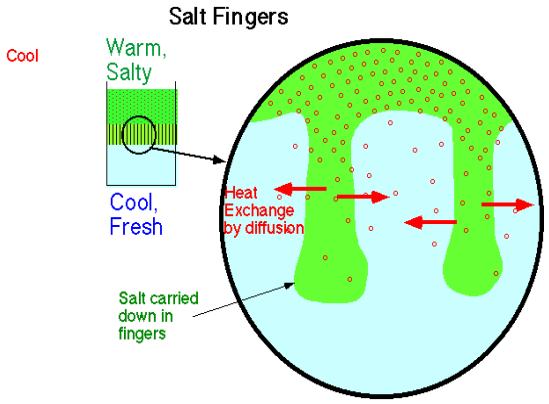

Figure 2. Salt Fingers. Fingers of salty and cooler water extend downward from the interface due to the difference in diffusivity rates of heat and salt. (After Ruddick, 1997)

2. Diffusive Convection Regime

While salt fingering has been a subject of considerable interest since its discovery, the diffusive convection, on the other hand, historically received less attention. One of the reasons is related to its prevalence in high-latitude locations, where field programs are more demanding. Nevertheless, clear signatures of the diffusive convection have been observed and recorded (Kelley, 1990; Padman &

Dillon, 1987). This study is focused on the diffusive convection regime where cold and fresh water overlies relatively warm and salty water.

To understand the dynamics of diffusive convection, imagine displacing a parcel of warm and salty water, as illustrated in Figure 3. This time, it is displaced upward across the thin interface into cooler and fresher water. As expected, the parcel of water quickly diffuses the heat it carried with it to its new surroundings and slowly releases its salt. However, since the parcel of water has now cooled and has not lost much of its salinity, it sinks across the interface and overshoots its original starting point due to increased density due to heat loss. As it returns to warmer waters, it once again gains heat and eventually will rise above the interface to once again lose its heat. This over-stable process is known as oscillatory diffusive convection.

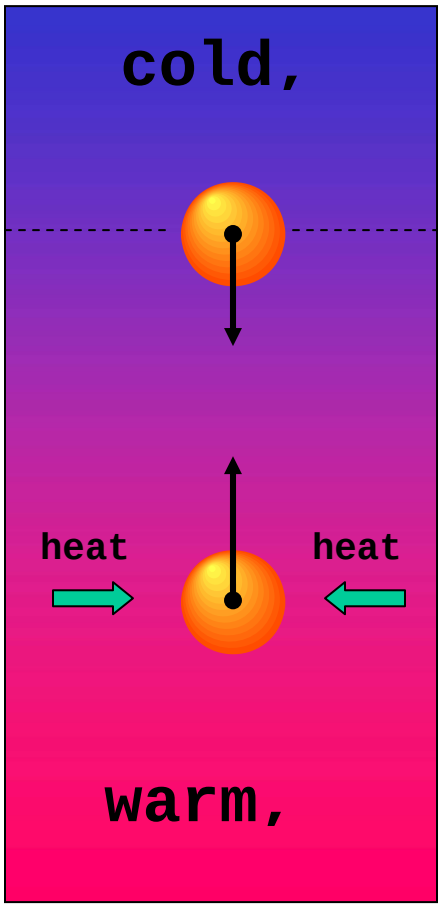

Figure 3. Oscillatory regime. The fluid parcel is caught oscillating up and down shuttling heat upward.

This form of instability is, however, of limited interest, since diffusive oscillations are eventually replaced by the quasi-steady patterns, characterized by the layered distribution of temperature and salinity (Prikasky, 2007). Therefore, most commonly found in the Arctic is the mode of diffusive layering. Well-mixed layers separated by sharp diffusive interfaces are responsible for stair-like appearance the temperature profiles in the central Arctic thermocline. Such profiles are referred to as thermohaline staircases. Figure 4, below, depicts one of the steps in the staircase where a layer of cold and fresh water lies

over more warm and salty water. A warm layer diffuses heat through the thin interfacial layer, immediately above it. Particles located just above the interface warm up and rise, whereas particles immediately below the interface cool off and sink. The resulting convection cells above and below the interface maintain a homogeneous distribution of T-S in each layer.

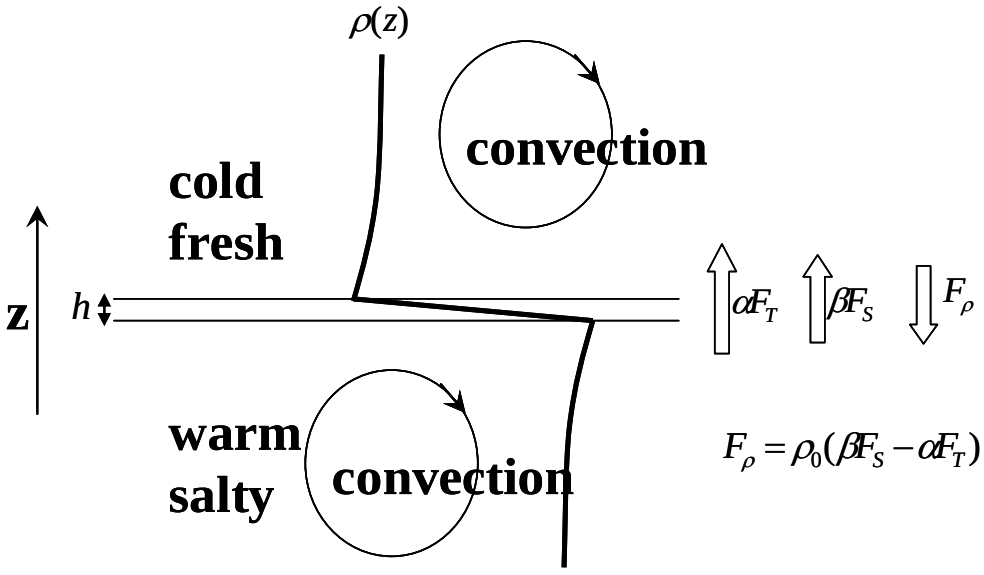

Figure 4. Typical thermohaline staircase. Heat convects upward through the interface while the salt transport is limited by its lower molecular diffusivity.

Diffusive staircases are observed where the thermocline has a negative temperature gradient. Heat is transferred upward through a sequence of adjacent steps in the staircase. The numerical model used in this study makes use of periodic boundary conditions illustrated in Figure 5. These boundary conditions offer a fairly realistic

representation of the mixing that occurs in nature, particularly in comparison to the lab experiments described above.

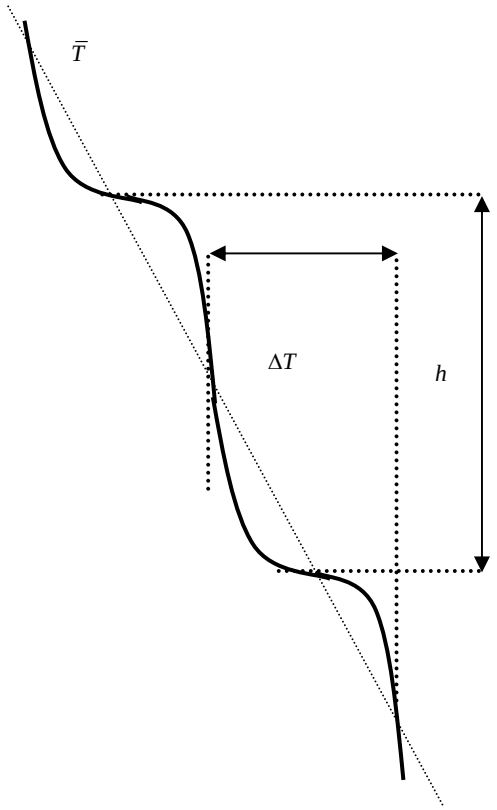

Figure 5. Schematic diagram illustrating the infinite series of identical steps. In following discussion, the temperature variation across each step (ΔT)is defined as a difference in temperature between the centers of two adjacent layers (After Radko, 2005).

III. PRELIMINARY CALCULATIONS

A. ICE-TETHERED PROFILER

The Ice-Tethered Profiler (ITP) was designed for deployment on the perennial sea ice in the polar oceans. It brings together two main types of oceanographic sampling technologies; the mooring station and the drifter. The marriage of these two technologies allows the sampling apparatus to remain above the ocean surface in constant contact with shore facilities while also drifting about the ocean along with the ice floe it is moored to. The ITP has three main components: a surface subsystem; a weighted, plastic-jacketed wire tether suspended from the surface unit; and a profiler that travels up and down the jacketed wire via a traction drive (see Table 1 further ITP specifications). The profiler reports its findings to the surface unit using an inductive modem after each one-way traverse. From the surface unit, this data is then transferred to shore-based facilities using an Iridium transmitter.

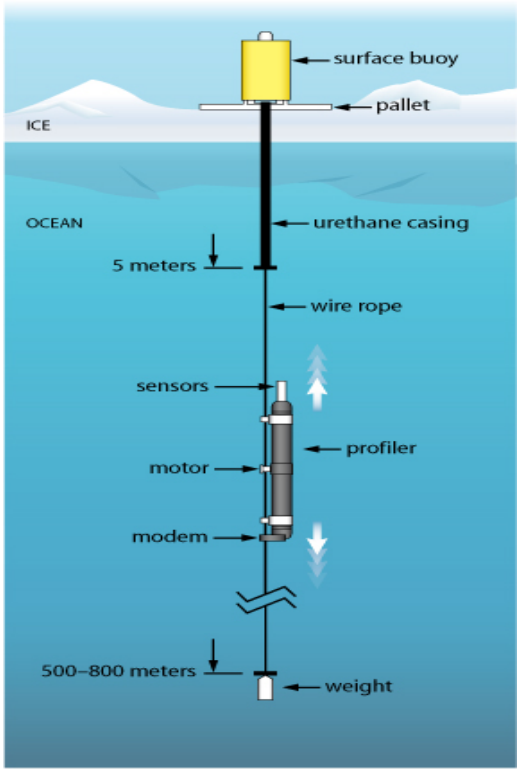

Figure 6. Ice-Tethered Profiler schematic. Illustration obtained from WHOI ITP website: http://www.whoi.edu/oceanus/viewArticle

Size	Surface unit—100 cm in length, 66 cm in diameter
	Underwater profiling unit—123 cm in length, 23 cm in diameter (cylindrical section diameter is 15 cm); fits through 25-cm-diameter ice hole
Tether length	Up to 800 m
Mass	Surface unit—70 kg
	Profiler—30 kg
	Tether (800 m)—250 kg
	Termination weight—114 kg
Profiling range	Approximately 1 500 000 m on standard battery pack
Endurance	2.5 to 3 yr returning two 750-m (one way) profiles per day (~2000 total)
Surface unit temperature specification	Operates to −35°C for prototypes, resumes full operation after experiencing temperatures down to −48°C
Sensors	Sea-Bird 41-CP CTD
	Dissolved oxygen, photosynthetically available radiation (PAR), chlorophyll fluorescence, optical backscatter, and carbonic dissolved organic matter (CDOM) in development
Telemetry	Sea-Bird, Inc., inductive link from profiler to surface unit;
	Iridium link to shore using dial-up data modem
Data telemetry	Typically 50 Kbytes per profile (totaling 100 Mbytes over 3 yr)
Power	Lithium BCX DD battery packs; 3300 Wh in surface package (after derating for temperature)
	2500 Wh in profiler

Table 1. Specifications of the ITP hardware and telemetry system. (After Krishfield et al., 2008)

Data received at the WHOI shore facility are then processed and made publicly available on the ITP internet website (http://www.whoi.edu/itp) as soon as they are received (Krishfield et al., 2008).

There are three general types of data sets that are readily available for download on the WHOI website: Level 1 Raw Data, Level 2 Real Time Data, and Level 3 Archive Data. Level 1 Raw Data is simply raw sensor and engineering data acquired by the profilers. The binary data are unpacked and reformatted into Matlab, one file per profile. Level 2 Real Time Data incorporates filtered location data and interpolated to the start times of each profile. The scientific and engineering data are then averaged in 2-db bins. No sensor response corrections, calibrations or editing are made in Level 2 Real Time Data, other than the internal calibrations of the CTD instruments. Finally, Level 3 Archive Data represents the best estimates of the ocean properties. The data have had sensor response corrections, regional conductivity adjustments based on historical data, and edits performed. These corrections and adjustments are not made until the ITP has completed its mission (Krishfield et al., 2008).

B. DATA ANALYSIS

Data sets from ITPs 1, 2, 3 and 5 were chosen based on the tracks they ended up traveling over while they were deployed. Figure 7 is a graphic taken from the WHOI ITP website and it depicts the area the four ITPs covered.

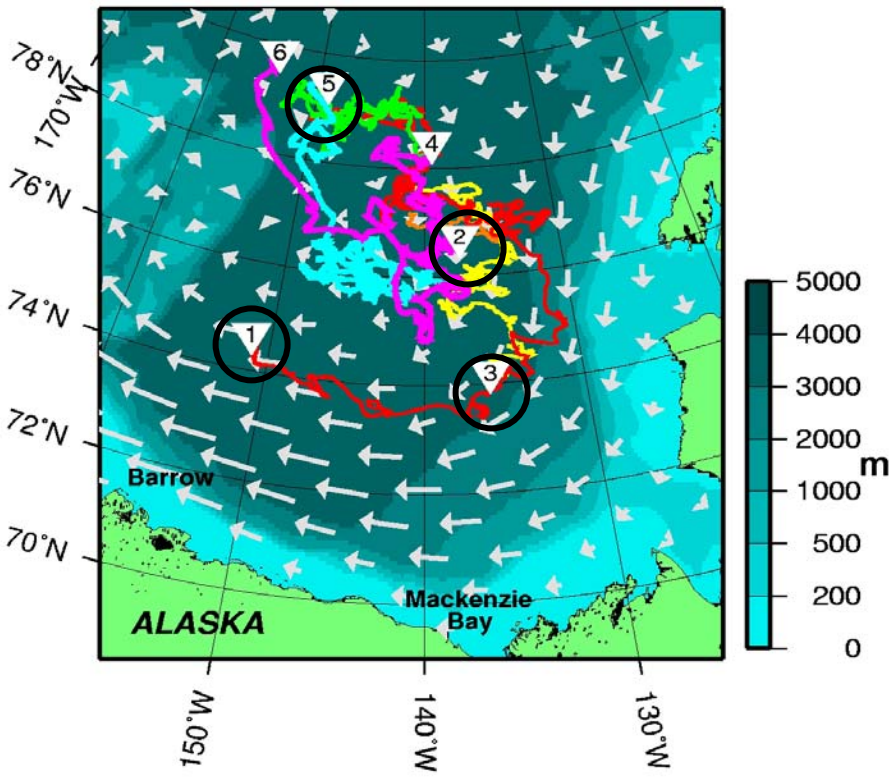

Figure 7. ITP tracks through the Beaufort Gyre. Illustration obtained from WHOI ITP website: http://www.whoi.edu/page.do?pid=23099

Matlab routines were written to process the data. First, temperature (Figure 8) and salinity profiles (Figure 9) were plotted for each ITP. To identify the range of depths at which the preponderance of thermohaline steps existed, temperature versus depth was plotted in groups of 20-50 profiles per plot as shown in Figure 10. Next, layer interfaces were identified utilizing Matlab script which looked for a maximum change in temperature. Once the interfaces were identified, the script then identified the corresponding temperature, salinity and depth with each interface and marked the midpoints of each step shown in

Figure 11. These quantities were then used to calculate the background density ratio, R_ρ, using equation (5) for each profile recorded:

$$R_\rho = \frac{\beta \Delta S}{\alpha \Delta T}, \tag{5}$$

where β is the coefficient of saline contraction, α is the coefficient of thermal expansion, and ΔS and ΔT are the variations in salinity and temperature across each step, respectively. Both β and α were calculated using the Matlab seawater toolbox.

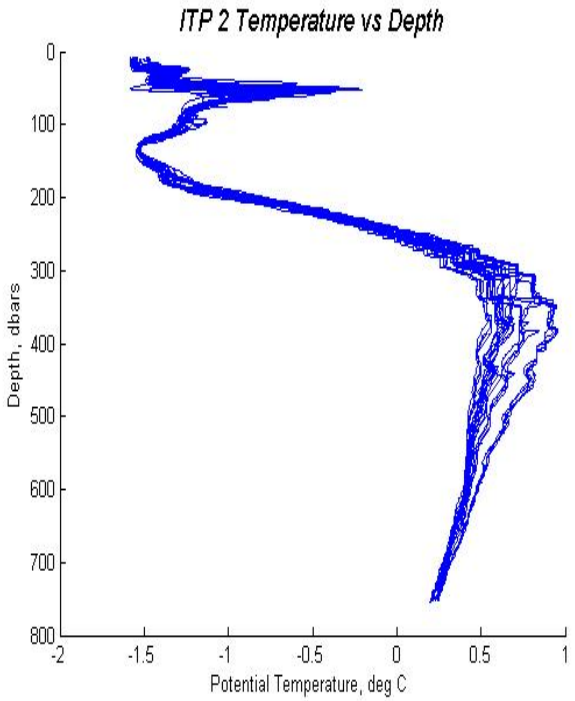

Figure 8. Temperature profile for ITP2. 244 profiles depicted.

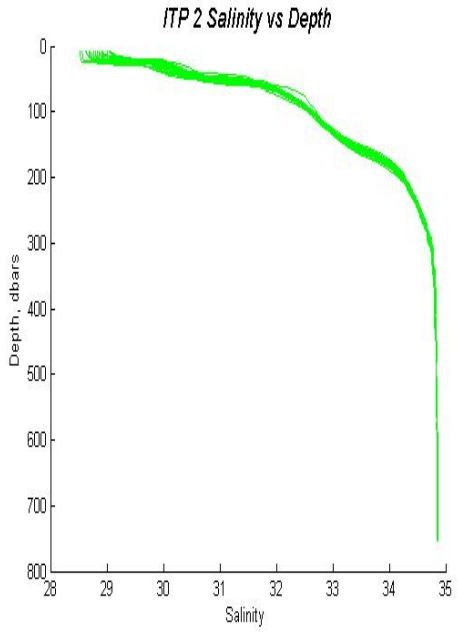

Figure 9. Salinity profile for ITP 2. 244 profiles depicted.

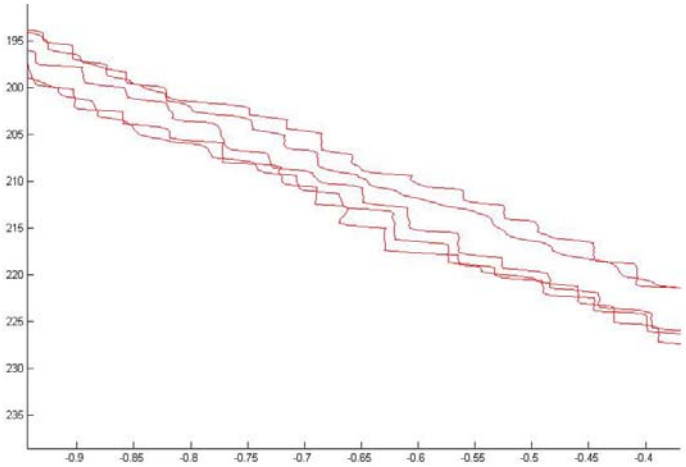

Figure 10. Typical thermohaline staircase structure for ITP2.

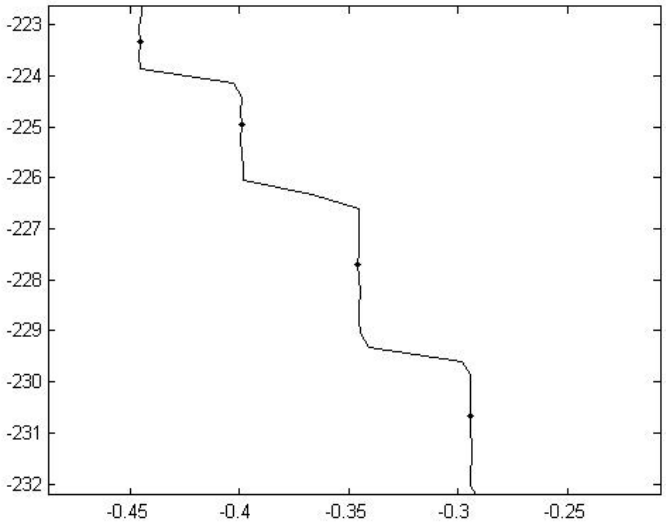

Figure 11. Individual profile within ITP 2 data set. Marker indicates the midpoint of each step as identified by routine written in Matlab.

Table 2 summarizes the parameters that quantify the thermohaline staircases within the Beaufort Gyre. Of most importance is the calculation of Density Ratio. This quantity is a measure of intensity of diffusive convection and is essential for the correct estimate of heat fluxes using a numerical model.

Profiler	Mean Density Ratio	Mean Step Height, meters	Mean Temperature Gradient
ITP 1	4.87 +/- 1.72	2.70 +/- 1.02	0.0164 +/- 0.0054
ITP 2	4.81 +/- 1.52	2.54 +/- 0.80	0.0165 +/- 0.0068
ITP 3	5.43 +/- 1.70	2.42 +/- 0.77	0.0160 +/- 0.0102
ITP 5	4.59 +/- 1.33	2.46 +/- 0.81	0.0158 +/- 0.0053

Table 2. Mean density, step height, and temperature gradient within the Beaufort Gyre.

THIS PAGE INTENTIONALLY LEFT BLANK

IV. DIRECT NUMERICAL SIMULATIONS

A. MODEL DESCRIPTION

Direct Numerical Simulations was conducted in both two and three dimensions on Naval Postgraduate School (NPS) high-performance clusters, Anastasia and Kinglear, in addition to Department of Defense (DoD) supercomputer clusters, Babbage, Davinci, and Midnight. Low resolution model runs were set up on the NPS clusters dedicating only one processor per run. High-resolution runs committed 16 processors per run across the three DoD supercomputer clusters and NPS's Kinglear. Because of a wide range of spatial and temporal scales, numerical modeling of diffusive staircases represented a formidable computational challenge, particularly in three-dimensions, and required use of parallel architecture. The numerical model is a fully de-aliased pseudo-spectral FORTRAN code, described in Radko (2003), using the Message Passing Interface (MPI) for three dimensions. The numerical setup was based on Ice-Tethered Profiler observations (from the Beaufort Gyre Exploration Program led by Woods Hole Oceanographic Institute) and the results were compared with existing models. The two-dimensional study examined the diffusive convection in the horizontal (x) and vertical (z).

Following Radko and Stern (1999), temperature and salinity fields are decomposed into the linear basic state $(\overline{T},\overline{S})$ and perturbations (T,S). The Boussinesq equations of motion are non-dimensionalized using $\mathrm{d} = (\kappa_T \nu / g\alpha\overline{T_z})^{\frac{1}{4}}$ as the

length scale, $\mathrm{v}=\frac{\kappa_T}{\mathrm{d}}$ the velocity scale, $\mathrm{t}=\frac{\mathrm{d}^2}{\kappa_T}$ as the time scale, where κ_T is the molecular diffusivity of heat, ν is the kinematic viscosity, g is the gravitational acceleration, α is the coefficient of thermal expansion, T_z is the temperature gradient and $\alpha T_z \mathrm{d}$ is the scale for both temperature and salinity perturbations resulting in

$$\left.\begin{aligned} &\frac{1}{\mathrm{Pr}}\frac{d\mathrm{v}}{dt} = -\nabla p + \nabla^2 \mathrm{v} + (T-S)k, \\ &\nabla \cdot \mathrm{v} = 0, \\ &\frac{dT}{dt} - \mathrm{w} = \nabla^2 T, \\ &\frac{dS}{dt} - R_\rho \mathrm{w} = \tau \nabla^2 S, \end{aligned}\right\} \qquad (2)$$

where $\mathrm{Pr}=\nu/\kappa_T$ =13 is the Prandtl number, $\tau=\kappa_S/\kappa_T$ is the molecular diffusivity ratio (Lewis number), R_ρ is the background density ratio for the basic uniform S-T gradient, while v, T, and S are non-dimensional velocity, temperature, and salinity.

The non-dimensional and dimensional temperature fluxes are related by

$$F_{T\,\mathrm{dim}} = F_{T non-\mathrm{dim}} \kappa_T dT/dz \qquad (3)$$

and the corresponding heat flux is

$$F_{H\,\mathrm{dim}} = F_{T\,\mathrm{dim}}\, C_p \rho \qquad (4)$$

where C_p is the specific heat for sea water and ρ is the density of sea water. Substituting (3) into (4) yields the

conversion factor between the dimensional heat flux and non-dimensional temperature flux of $.0094 W/m^2$.

The strategy was to focus on two-dimensional simulations and compare the results to computationally accessible three-dimensional simulations. The ratio of three-dimensional heat fluxes to two dimensional heat fluxes would then be used to calibrate all two-dimensional simulations.

B. TWO-DIMENSIONAL SIMULATION

1. General Characteristics

In order to gain an understanding of the mechanism of diffusive layering and its dependencies on the governing parameters, two-dimensional simulations calculated heat fluxes as functions of background density ratio, ranging from 3 to 6, and Lewis numbers with ratios 1/200, 1/100, 1/50 and 1/25 creating a 4x4 matrix data set shown in Table 2. The simulation runs were initiated from a random computer-generated distribution of T and S. The grid size used in the initial 16 two dimensional runs was 2048x4096.

A typical evolutionary pattern observed in the two-dimensional simulations are shown in Figure 12. The two layered simulation is initiated at rest. Random noise gives the system a kick and initiates the diffusive process. Notice the huge spike in the very beginning of the simulation indicating the quick release of potential energy by the temperature field. As time increases the fluctuations in the heat fluxes eventually reach equilibrium. Mean heat fluxes were determined from the

equilibrated portion of the graph (typically achieved during last one-third of time record).

Figures 13, 14, 15 and 16 are successive full temperature field plots revealing the spatial structure of the diffusive convection. The two layered fluid is at rest initially, as shown in Figure 13. Figure 14 depicts signs of initial convective activity as the heat exchange begins to diffuse between the two layers at t=50 minutes.

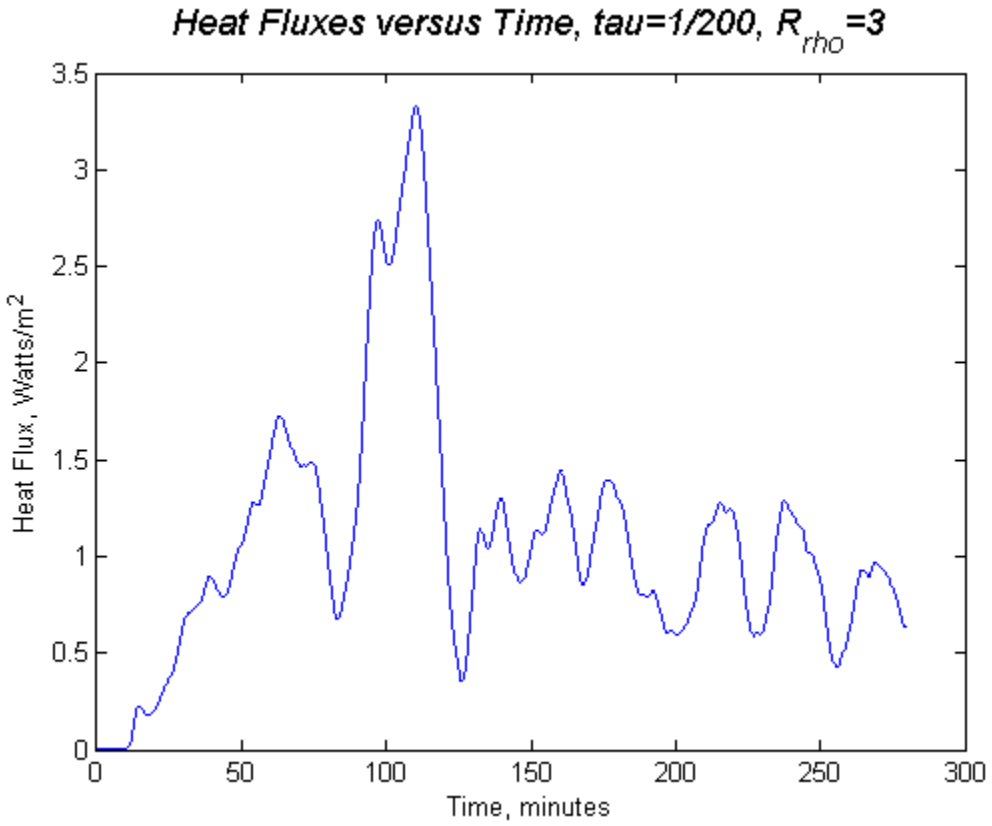

Figure 12. Typical two-dimensional plot of heat flux versus time.

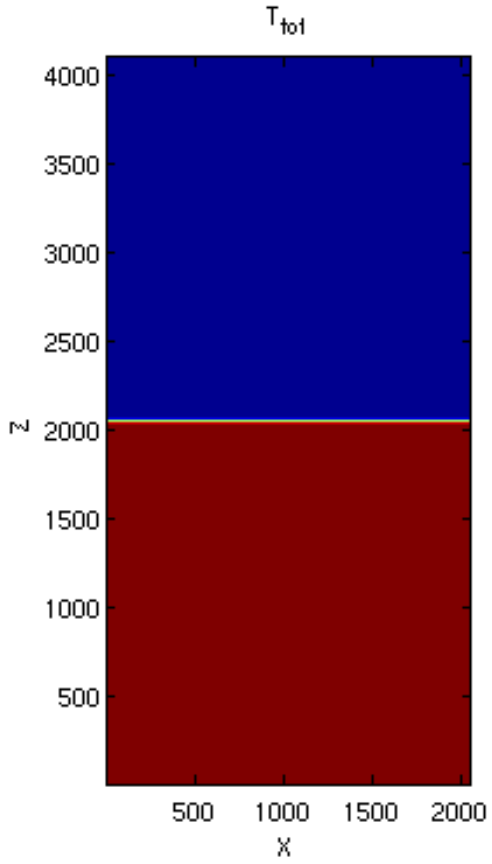

Figure 13. Two-dimensional temperature field. Plot is on XZ grid size of 2048x4096 at t=0 minutes. High values of T are shown in red. Low values in blue.

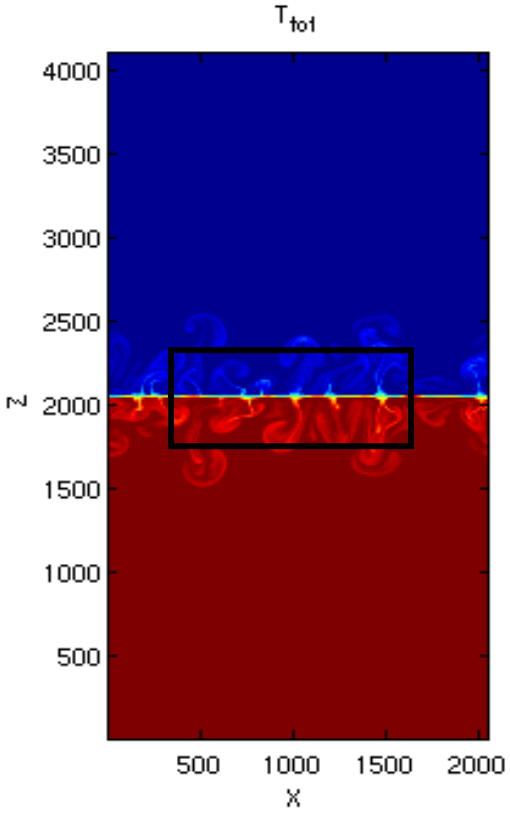

Figure 14. Two-dimensional temperature field. Plot is on XZ grid size of 2048x4096 at t=50 minutes. Convection plumes become visible in both layers. High values of T are shown in red. Low values in blue.

The heat signatures of active heat transport are clearly visible at t=200 minutes in Figure 15. This figure represents an enlarged view of the two fluid interface to show more detail of the dynamic event.

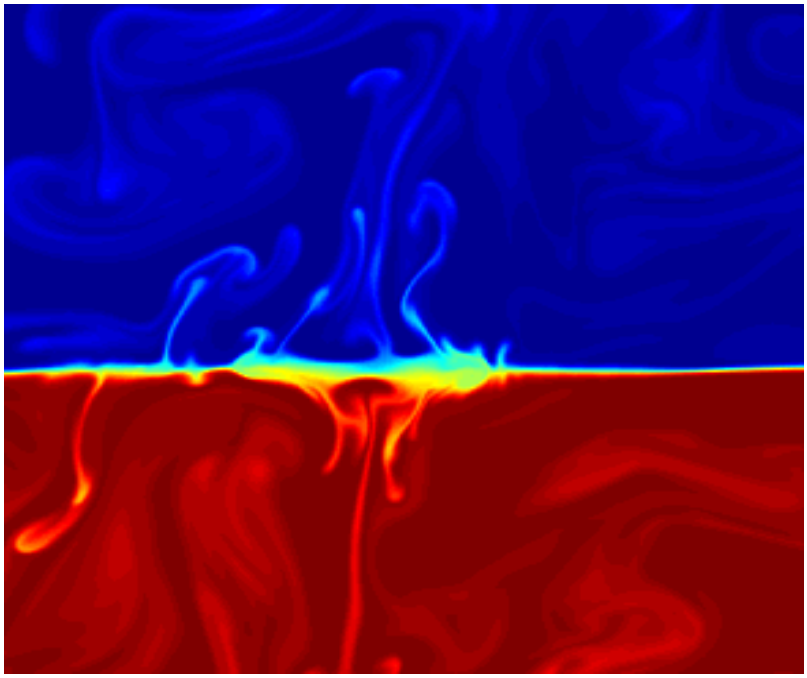

Figure 15. Two-dimensional temperature field at t=200 minutes. View is zoomed in on the interface to show more detail of convective dynamic. Temperature field is well mixed above and below the interface.

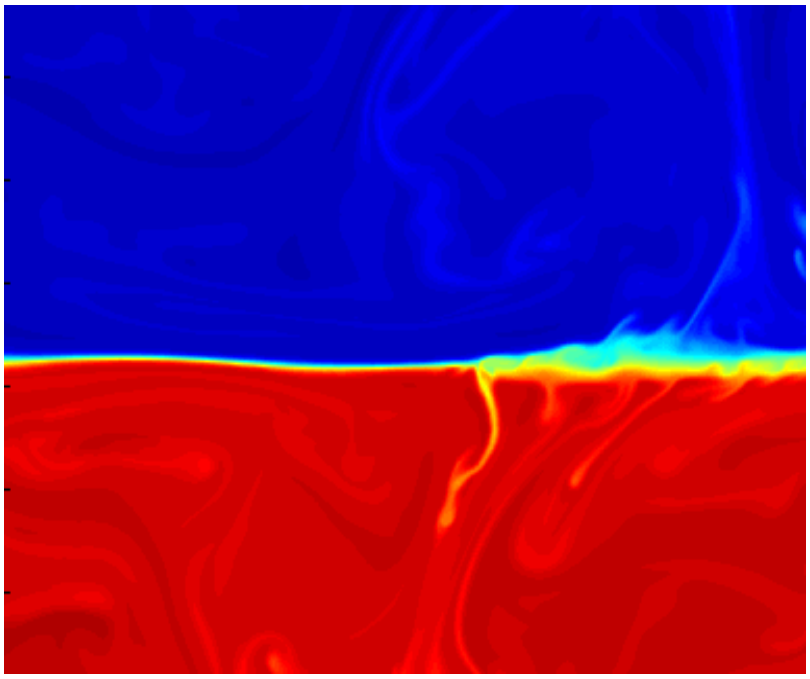

Figure 16. Two-dimensional temperature field plot at t=400 minutes. View is zoomed in on the interface to show more detail of convective dynamic. Interface is beginning to show signs of further convective activity with small plumes emanating from the right side of the picture.

2. Dependence of Fluxes on the Density Ratio

As indicated by equation (1), Turner suggests that heat fluxes are dependent on the density ratio for a fluid with a given temperature variation across the interface as deduced from the foregoing numerical experiments. Figure 17 illustrates this dependence on density ratio. As expected, heat fluxes decreased as the density ratio increased. In fact, heat fluxes were doubled when density ratio increased from R_ρ = 3 to R_ρ = 6.

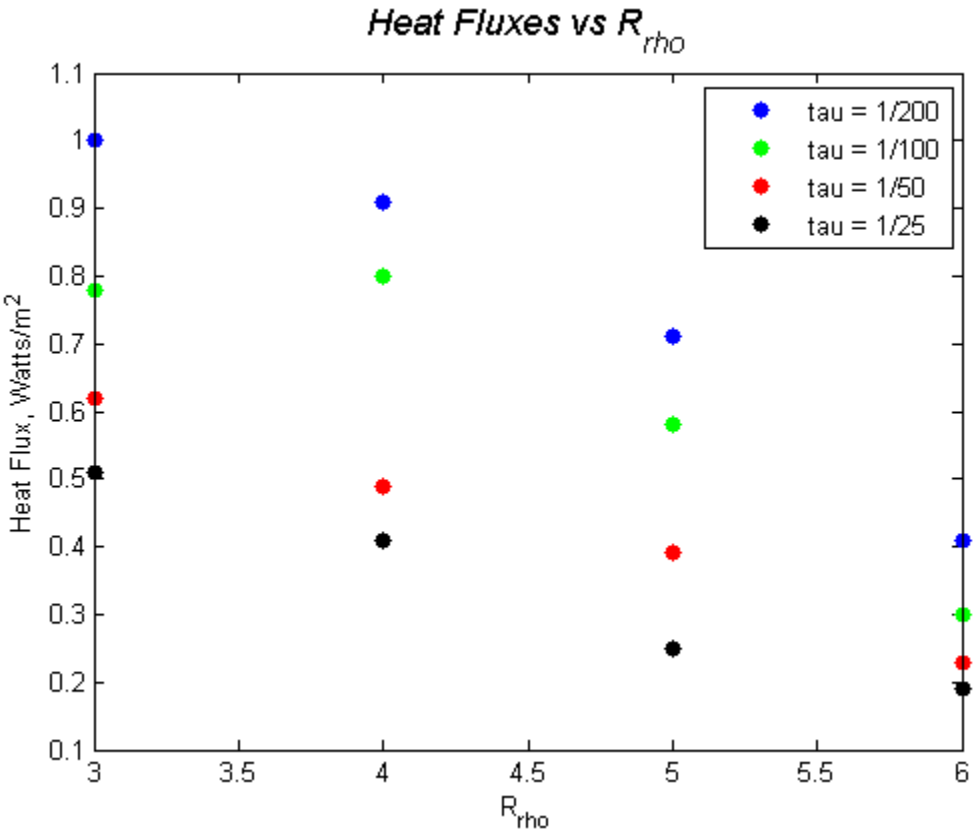

Figure 17. Two-dimensional heat flux versus density ratio. Heat fluxes decrease as density ratio increases.

3. Dependence of Fluxes on the Lewis Number

The Lewis number is a non-dimensional ratio between the diffusivities between salt and heat. A study conducted by Takao and Narusawa (1980) quantified the relationship of Lewis number and heat fluxes based on a series of laboratory experiments with substances of different molecular diffusivity ratios. They found that heat fluxes increased as the Lewis number decreased. This dependence on the Lewis number, although less pronounced, is also found in this study. Heat fluxes increased as Lewis number decreased over a range from τ=1/25 to τ=1/200 as depicted in Figure 18.

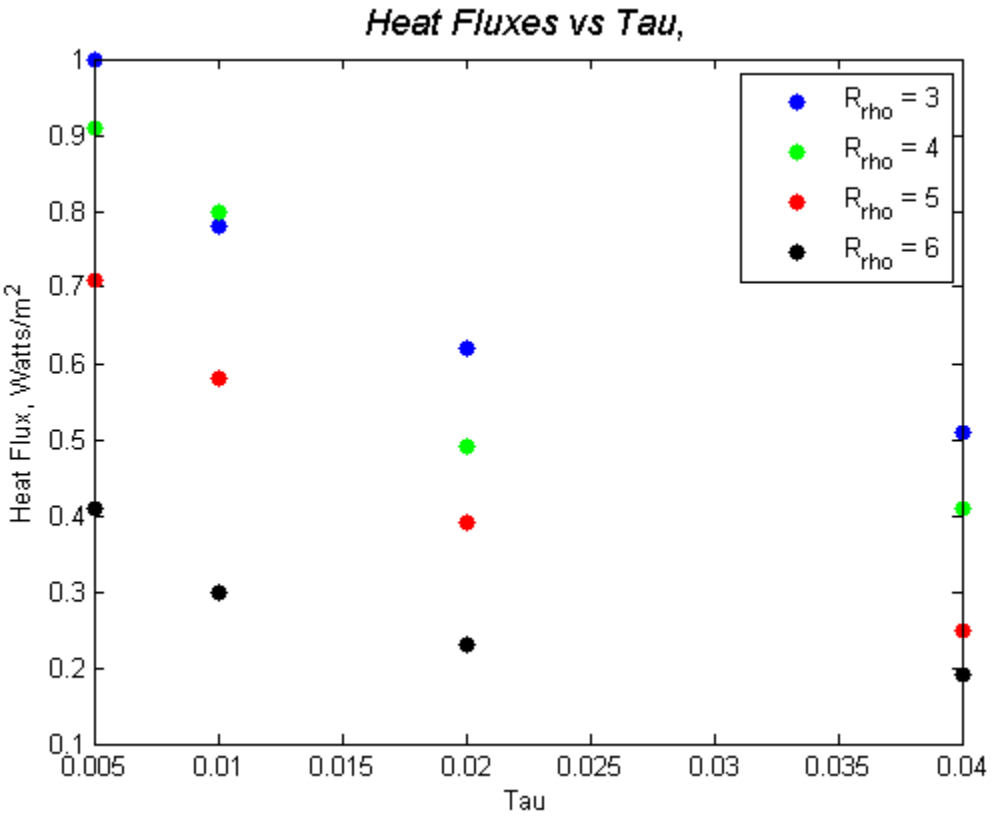

Figure 18. Two-dimensional heat flux versus Lewis number. Heat fluxes decrease as Lewis number increases.

The two-dimensional simulation results are summarized in Table 3. The results show that diffusive heat fluxes increase by a factor of two to three as the Lewis number decreases from 1/25 to 1/200. It should be noted that Lewis numbers on the order of 1/100 to 1/200 are typical for the ocean. As stated earlier in the paper, there is a general consensus that heat fluxes that are considerably less than $1 W/m^2$ are not significant enough to affect the Arctic Ocean surface heat budget. Here, the simulation consistently achieved heat fluxes on the order of $1 W/m^2$ for aforementioned density ratio and Lewis number ranges.

R_ρ / τ	3	4	5	6
1/200	1.1 W/m^2	0.78 W/m^2	0.62 W/m^2	0.51 W/m^2
1/100	0.91 W/m^2	0.80 W/m^2	0.49 W/m^2	0.40 W/m^2
1/50	0.71 W/m^2	0.58 W/m^2	0.39 W/m^2	0.25 W/m^2
1/25	0.41 W/m^2	0.30 W/m^2	0.23 W/m^2	0.19 W/m^2

Table 3. Two-dimensional diffusive heat flux as a function of density ratio and Lewis number.

C. THREE-DIMENSIONAL SIMULATION

In order to comply with the limits set by the available computing resources, a three-dimensional simulation was run with R_ρ= 6 and τ=1/10 was conducted and compared with the corresponding two-dimensional run. This Lewis number, τ=1/10, was chosen due to it being computationally accessible in the three-dimensional simulation. Choosing smaller Lewis numbers necessitated resolving the salt diffusivities at very fine scales, which proved to be computationally prohibitive. A grid size of 256x512 and 256x256x512 were used for the additional two-dimensional and comparable three-dimensional runs, respectively.

Figure 19 illustrates the simulation conducted in three-dimensions. Again, the simulation begins at rest and is perturbed by small amplitude random noise. The system had an initial spike and began to settle down as time increased.

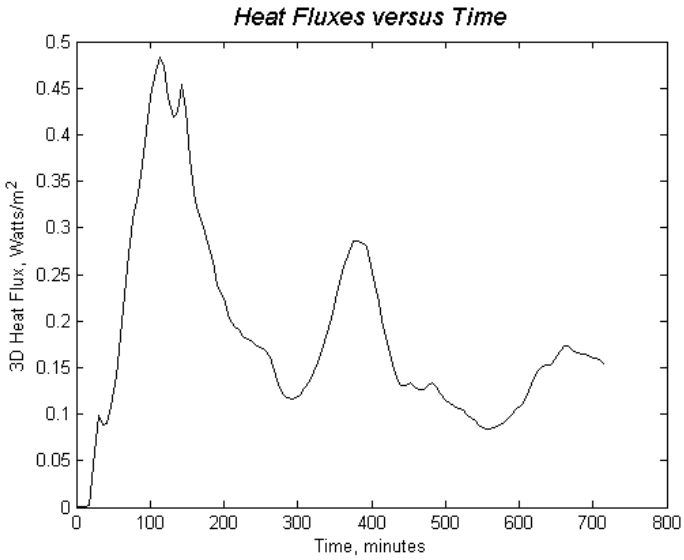

Figure 19. Three-dimensional heat flux versus time. R_ρ = 6 and τ =1/10

Figures 20 to 23 illustrate the evolutionary process of the temperature field in three-dimensions. Notice the "worm-like" patterns in the horizontal plane of Figure 21 indicating regions of convective plumes. These patterns have grown into larger strands of relatively cooler temperatures surrounded by pools of higher temperatures indicating areas of high and low heat flux, respectively.

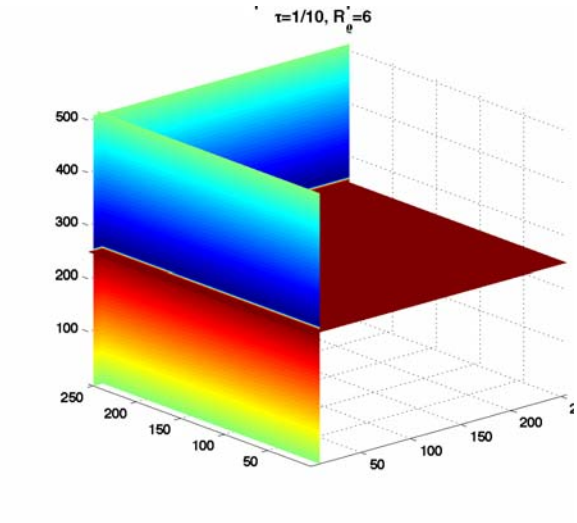

Figure 20. Three-dimensional temperature field plotted on XYZ grid size of 256x256x512 at t=0 minutes. High values of T are shown in red. Low values in blue.

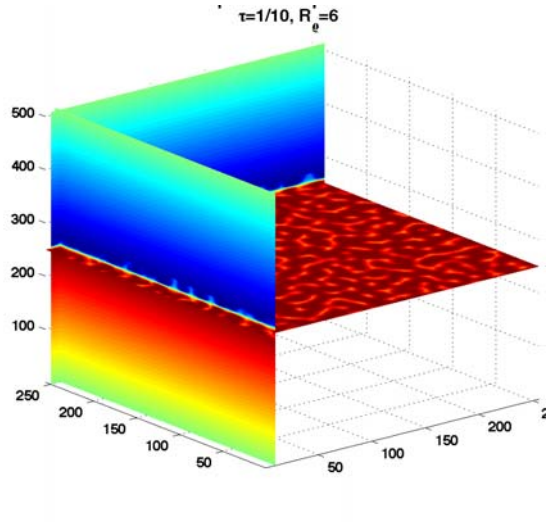

Figure 21. Three-dimensional temperature field plotted on XYZ grid size of 256x256x512 at t=70 minutes. Convection plumes become visible on vertical panels and are indicated by lighter “worm-like” patterns in the horizontal plane. High values of T are shown in red. Low values in blue.

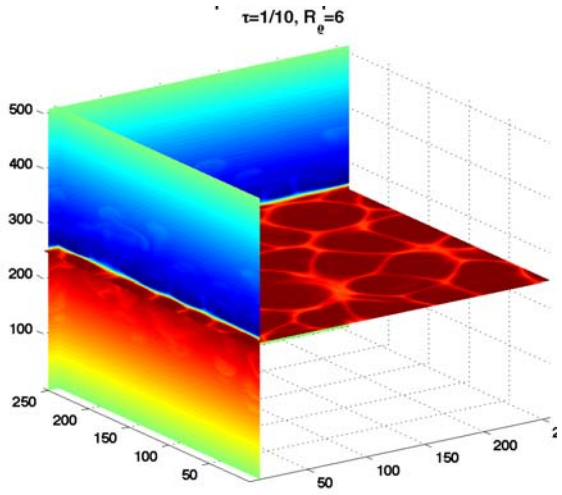

Figure 22. Three-dimensional temperature field plotted on XYZ grid size of 256x256x512 at t=500 minutes. Plumes are beginning to dissipate into mixing region above and below the layer. High values of T are shown in red. Low values in blue.

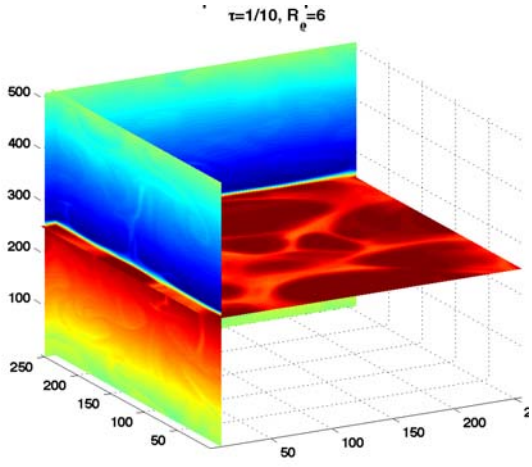

Figure 23. Three-dimensional temperature field plotted on XYZ grid size of 256x256x512 at t=700 minutes. The temperature field is now well mixed above and below the interface. High values of T are shown in red. Low values in blue.

D. CALIBRATION PROCEDURES

Resolving scale of finer detail becomes the issue when attempting to realistically model the ocean in three-dimensions. Lewis numbers on the order of τ=1/200 to τ=1/50 proved to be computationally difficult. However, this range of Lewis numbers is more accessible when simulated in two-dimensions. Figure 24 illustrates a 2-dimensional plot of heat fluxes utilizing the same input values, R_ρ= 6 and τ=1/10, used in the three-dimensional run.

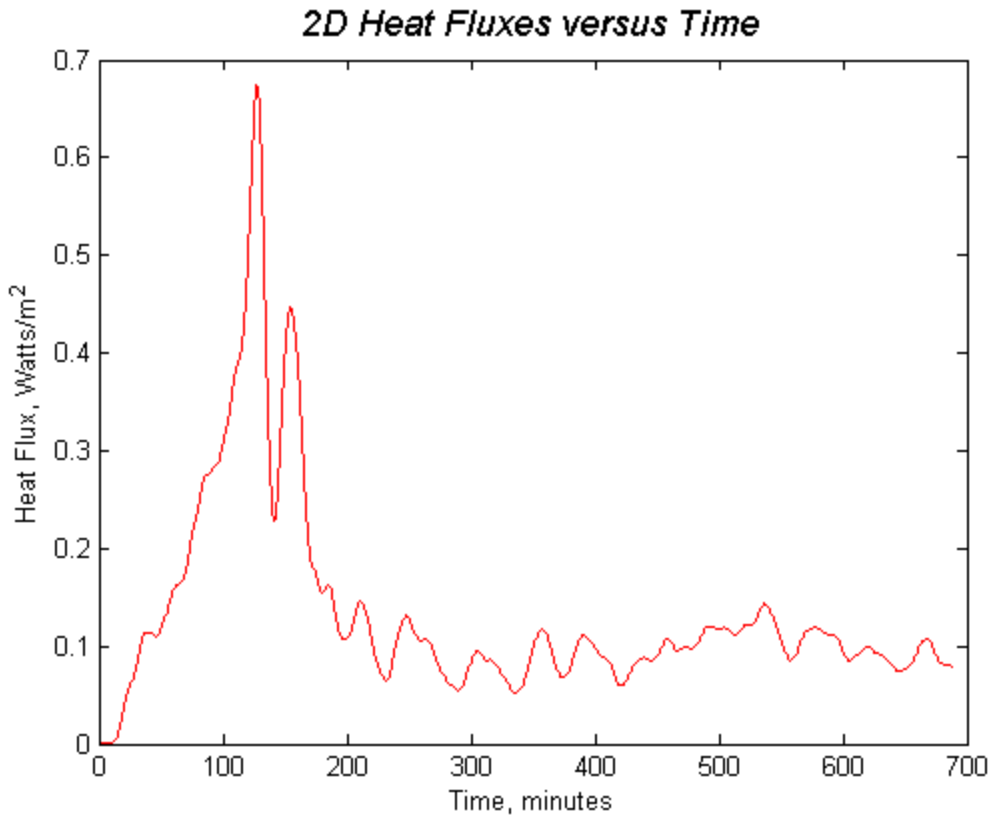

Figure 24. Two-dimensional heat flux versus time. R_ρ= 6 and τ=1/10.

Figure 25 presents a superposition of two-dimensional and three-dimensional simulations in Figures 23 and 24 and shows how heat fluxes simulated in two-dimensions compares to those calculated in three-dimensions. The mean value for the two-dimensional case was $0.1 W/m^2$, while the three-dimensional case was larger by 50%. Given this ratio of 1.5 and assuming it is valid for lower values of Lewis numbers in two-dimensions, Table 4 indicates the calibrated values for density ratios between 3 and 6 with a Lewis number of 1/200.

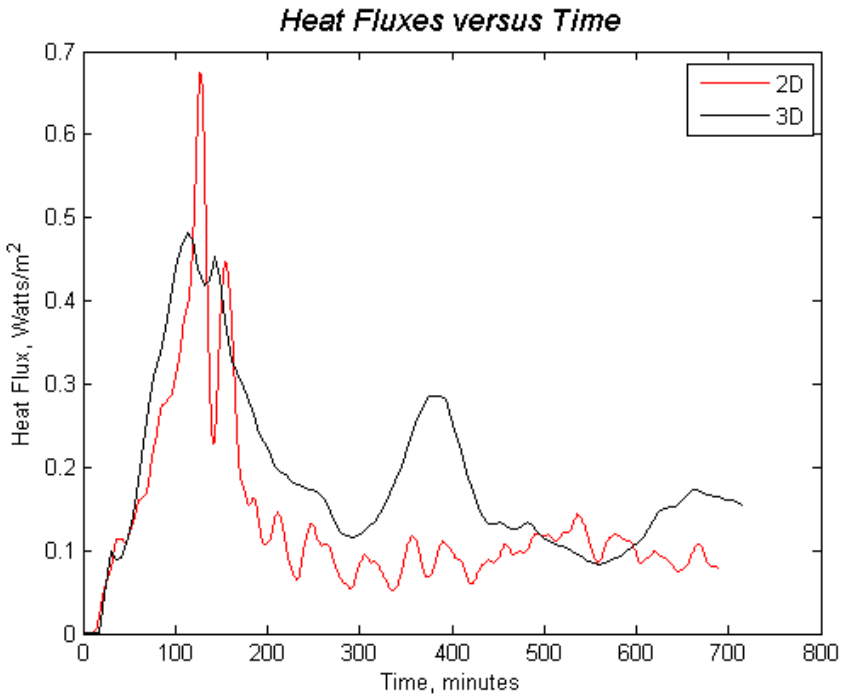

Figure 25. Comparison of two-dimensional heat flux with three-dimensional heat flux.

R_ρ / τ	3	4	5	6
1/200	1.1 W/m^2	0.78 W/m^2	0.62 W/m^2	0.51 W/m^2
1/200 Calibrated	1.65 W/m^2	1.17 W/m^2	0.93 W/m^2	0.77 W/m^2

Table 4. Two-dimensional diffusive heat flux as a function of density ratio and Lewis number 1/200. Calibrated values are 50% larger than the original based on the comparison of two-dimensional and three-dimensional simulations.

E. COMPARISON WITH LABORATORY EXPERIMENTS

In order to more fully explain the difference in fluxes using numerical simulations and the earlier estimates in Kelley (1990) derived from laboratory experiments, we now examine the lab-based flux laws directly. In particular, we turn our attention to the non-dimensional coefficient C of Turner's 4/3 flux law, equation (1). In Figure 26, we present the estimates of the non-dimensional factor C based on the numerical experiments in Table 4, superimposed on the earlier laboratory estimates. Numerical simulations produced values of C that were two to ten times larger than those achieved in laboratories. Again, this should raise the question as to the relevance of the lab based flux laws in application to the Arctic staircases.

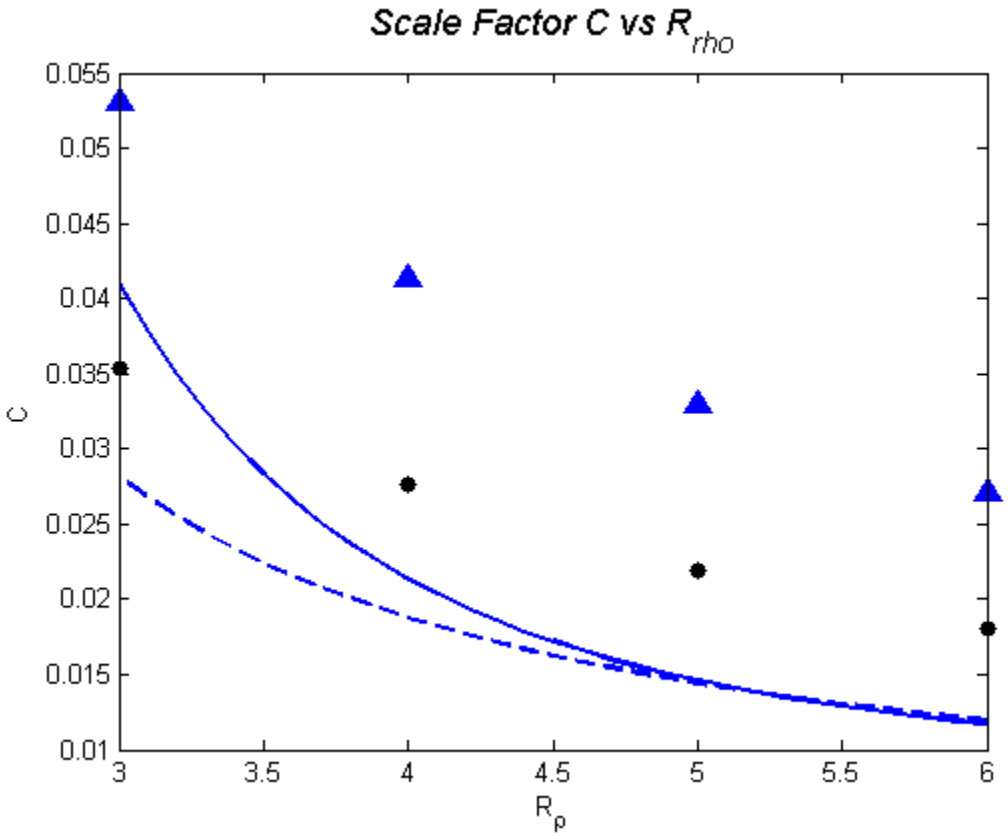

Figure 26. Non-dimensional coefficient of the 4/3 flux law $C(R_\rho)$ from equation (1). Data sources are indicated as follows: dashed Kelley (1990), solid Marmarino & Caldwell (1976), circles two-dimensional simulation, and triangles two-dimensional values scaled by three-dimensional simulation.

V. CONCLUSIONS AND RECOMMENDATIONS FOR FUTURE WORK

The double-diffusive estimates of the heat transport by convection in the Arctic are highly controversial. Laboratory-based estimates suggest that the vertical heat fluxes through the thermohaline staircases of the thermocline are typically on the order of $0.1 W/m^2$ (Timmermans, 2008; Padman & Dillon, 1987). This study indicates that these laboratory experiments underestimate the vertical heat fluxes and the numerical simulations exceed laboratory counterparts by an order of magnitude. Why such a large difference in values? It is my opinion that the laboratory experiments do not correctly model the ocean environment and therefore cannot accurately predict their vertical heat fluxes. Laboratory experiments are conducted in small tanks that have rigid boundaries, quite different parameter ranges and are very susceptible to experimental errors. Numerical modeling avoids many of issues, allowing vertical fluxes to pass through periodical boundaries, providing a more realistic model of the oceanic conditions. Heat fluxes in this study were found to be on the order of $1 W/m^2$ indicating that heat fluxes that arise from the Arctic thermocline are indeed significant and may play a role in the Arctic heat budget.

The analysis in this thesis warrants future work on this subject. Increasing the resolution of the model can imitate nature even more and provide more realistic results. Engaging in the inverse modeling of the Arctic staircases will resolve the controversy caused by the disagreement of different approaches. A further study to develop

quantitative analytical models of diffusive layering will help us better understand the nature of the diffusive convection. Finally, push the limits of modeling in three-dimensions to include lower Lewis numbers and adding in a horizontal T-S gradient to, again, better simulate nature.

It is my hope that these findings will cause the scientific community to re-evaluate their methods and simulate further research in this field of study. Only then can the challenge set by Admiral Gove be met, improving our prediction models and thereby improving our military's ability to improve our national security.

LIST OF REFERENCES

Gove, D. (2009). Arctic Melt: Reopening a Naval Frontier. Proceedings Magazine, 135. http://www.usni.org/magazines/proceedings/story.asp, accessed February 11, 2009.

Kelley, D. E. (1990). Fluxes through diffusive staircases: A new formulation. *Journal of Geophysical Research,* 95, 3365-3371.

Kraus, E., & Businger, J. (1994). *Atmosphere-ocean Interaction.* Oxford University Press, Inc., New York.

Krishfield, R., Toole, J., Proshutinsky, A., & Timmermans, M.-L. (2008). Automated Ice Tethered Profilers for seawater observations under pack ice in all seasons. *Journal of Atmospheric and Oceanic Technology*, 25, 2091-2105.

Marmorino, G. O. & Caldwell, D. R. (1976). Heat and salt transport through a diffusive thermohaline interface. *Deep-Sea Res.*, 23, 59-67.

Molemaker, M. J. & Dijkstra, H. A. (1997). The formation and evolution of a diffusive interface. *Journal of Fluid Mechanics,* 331, 199-229.

National Research Council, (2004). Abrupt climate change: Inevitable Surprises. Report in Brief. http://dels.nas.edu/dels/rpt_briefs/abrupt_climate_change_final.pdf, accessed March 3, 2009.

Padman, L., & Dillon, T. M. (1987). Vertical heat fluxes through the Beaufort Sea thermohaline staircase. *J. of Geophysical Res.*, 92, 10799-10806.

Prikasky, I. (2007). Direct numerical simulations of the oscillatory diffusive convection and assessment of its climatologic impact. Master's thesis, Naval Postgraduate School, Monterey, CA.

Radko, T., & Stern, M. E. (1999). Salt fingers in three dimensions. *J. of Mar. Res.*, 57, 471-502.

Radko, T. (2003). A mechanism for layer formation in a double-diffusive fluid. *Journal of Fluid Mechanics*, 497, 365-380.

Radko, T. (2005). What determines the thickness of layers in a thermohaline staircase? *Journal of Fluid Mechanics,* 523, 79-98.

Ruddick, B. R. (1983). A practical indicator of the stability of the water column to double-diffusive activity. *Deep-Sea Res*., 30, 1105-1107.

Ruddick, B. R. (1997). Differential fluxes of heat and salt: Implications for circulation and ecosystem modeling. *Oceanography*, 10, 3, 122-127.

Takao, S., & Narusawa, U. (1980). An experimental study of heat and mass transfer across a diffusive interface. *International Journal of Heat and Mass Transfer*, 23, 1283-1285.

Timmermans, M. L., Toole, J., Krishfield, R., & Winsor, P. (2008). Ice-Tethered Profiler observations of the double-diffusive staircase in the Canada Basin thermocline. *Journal of Geophysical Res.*, 113, C00A02, doi:10.1029/2008JC004829.

Turner, J. S., (1965). The coupled turbulent transports of salt and heat across a sharp density interface. *International Journal of Heat and Mass Transfer*, 8, 759-767.

Turner, J. S., (1973). *Buoyancy Effects in Fluids*. Cambridge University Press, New York.

United States Environmental Protection Agency, (2009). Polar Regions. http://www.epa.gov/climatechange/effects/polarregions.html, accessed March 3, 2009.

You, Y. (2002). A global ocean climatological atlas of the Turner angle: Implications for double-diffusion and water-mass structure. *Deep-Sea Res.*, 49, 2075-2093.

Woods Hole Oceanographic Institute, (2007). A new way to monitor changes in the Arctic. http://www.whoi.edu/oceanus/viewArticle.do?id=33006, accessed March 3, 2009.

THIS PAGE INTENTIONALLY LEFT BLANK

INITIAL DISTRIBUTION LIST

1. Defense Technical Information Center
   Ft. Belvoir, Virginia

2. Dudley Knox Library
   Naval Postgraduate School
   Monterey, California

3. Dr. Jeff Paduan
   Naval Postgraduate School
   Monterey, California

4. Dr. Timour Radko
   Naval Postgraduate School
   Monterey, California